Desalination and Water Treatment
www.deswater.com
doi: 10.5004/dwt.2023.29628

296 (2023) 49–59
June

Experimental and analysis study on removal of furfural in synthetic refinery wastewater using an agricultural waste-based modified adsorbent

Luma H. Mahmood[a], Mohammad F. Abid[b,*], Adnan A. AbdulRazak[a], Bashar J. Kadhim[a], Ibrahim N. Abdulla[b]

[a]*Department of Chemical Engineering, University of Technology, Baghdad, Iraq, email: 80152@uotechnology.edu.iq (L.H. Mahmood), 80036@uotechnology.edu.iq (A.A. AbdulRazak), bashar.j.kadhim@uotechnology.edu.iq (B.J. Kadhim)*
[b]*Department of Petroleum and Gas Refining Engineering, Al-Turath University College, Baghdad, Iraq, emails: mohammad.fadhil@turath.edu.iq (M.F. Abid), ibrahim.najim@turath.edu.iq (I.N. Abdulla)*

Received 5 January 2023; Accepted 14 May 2023

ABSTRACT

The current study was conducted to estimate and identify Fe-doped activated carbon synthesized from empty date palm bunch fibers that may be used for furfural efficient removal. The prepared adsorbent was identified by scanning electron microscopy, X-ray diffraction, and Fourier-transform infrared spectroscopy techniques. The capability of the modified adsorbent for furfural elimination in synthetic wastewater of the Al-Doura oil refinery in Baghdad city was estimated through both kinetic and equilibrium studies with investigating the key parameters such as adsorbent loading, contact time, furfural loading, initial pH, and mixing speed. Experimental results showed that after 125 min of contact time a percentage removal efficiency of 80% and 58% with absorption capacities of 27.04 and 16.80 $mg \cdot g^{-1}$ was attained by using Fe-doped activated carbon, and activated carbon, respectively at optimum initial pH of 6. Results showed that the pseudo-first-order fitted well with the system kinetics. Moreover, the Langmuir isotherm model agreed well with the adsorption equilibrium system. The thermodynamic study revealed that the negative value of $\Delta G°$ marks the spontaneity and feasibility of the sorption operation. A regression model was developed for the percentage removal of furfural as a function of operating parameters with a correlation coefficient of 0.9875 and a standard of deviation = 1.18%.

Keywords: Agricultural wastes; Fe-doped activated carbon; Furfural; Synthetic wastewater; Kinetic study, Equilibrium study

1. Introduction

The existence of toxic pollutants such as solvents, hydrocarbons, metals, and a lot of other organics set free as outflowing from the petroleum and petrochemical industrial processes is generating significant menaces to the environment. Among the numerous components existing in the environment, furfural is utilized in a wide range in refineries and petrochemical industries, paper and pasteboard, and petroleum refining and is existing in their effluent water on the scale of 10–1,500 ppm [1,2]. Furfural is classified as aromatic aldehydes that are dissolvable in water and boiling at 161.8°C [3]. Exposure of humans to the concentricity of 1–15 ppm from furfural has resulted in headaches and the ruddiness of the eyes. Exposure to more concentricity results in pulmonary edema [4]. Various techniques have been considered in furfural elimination like biological, adsorption, photocatalytic, and exacting techniques [5–7]. Although, the more paramount of which are biological techniques and adsorption operation [8]. Published data have revealed that furfural biodegradation comprises both aerobic and anaerobic paths, which are costly. Moreover, under

* Corresponding author.

the effect of different variables and toxicity of furfural at high loadings, the utilization of this technique was making furfural degradation more difficult [9].

Activated carbon (AC) is abundant, cheap, has a large surface area, is re-generable, and has large pore capacity, and thus has shared immense, implementations [10]. However, commercial-AC has been showing expensive. So, there is a continuous search for an economical and accessible substance that may be instead of the commercially obtainable AC. On the other hand, AC can be gained widely from substances like agricultural wastes [11]. Enormous numbers of fruitful palm-dates trees are implanting in Iraq. Although, the remnant of the palm tree, particularly, the empty date palm bunch (EDB) has still not been entirely used. Abid et al. [12] investigated experimentally the production of glucose from the Iraqi EDB. Additionally, there are quite finite published data that have been done on the effectiveness of AC synthesized from Iraqi EDB fibers. The literature reported that AC materials enriched with various shapes of Fe_2O_3 or $Fe(OH)_2$ may display high capability for the elimination of many pollutants from wastewater [13–15]. Wang et al. [16] studied the adsorption mechanism of phosphate on iron-doped activated carbon. The authors suggested that the phosphate-carbon reaction could be dominated by a chemical adsorption mechanism through electro-static adsorption in the outer layer and chemical bond force in the inner layer. The authors revealed that AC/O-Fe has a higher phosphate removal capacity than AC-Fe, which could be attributed to its higher affinity toward phosphate probably due to the existence of the above-mentioned interactions. Moreover, the adsorption process was complex; chemical adsorption, surface mass transfer, and intraparticle diffusion were simultaneously occurring during the process and contribute to the adsorption mechanism.

Chatla et al. [17] studied the removal of Pb^{2+} ions by 5 wt.% Fe-doped AC. The authors reported that the process of Pb^{2+} ions removal was found as endothermic and spontaneous process as confirmed by the analysis of thermodynamic adsorption parameters. They revealed that both chemical and physical mechanisms participated in the adsorption process including electrostatic interactions, complexation, ion exchange and surface adsorption.

Soudani et al. [18] studied the synthesis of biochar from oak fruit shells using one-step pyrolysis at 700°C. The prepared biochar was used to remove Cu^{2+}, Cd^{2+}, and Zn^{2+} in an aqueous solution. The authors reported that the adsorption equilibrium metal ions onto biochar were reached after 4 h of contact time with a removal efficiency of 95.29%, 94.63%, and 82.99% for Cu^{2+}, Zn^{2+}, and Cd^{2+}, respectively. Praveen et al. [19] presented an overview of biochar synthesis and application for the removal of dyes in contaminated water. Their review integrates the recent works of literature to understand the biosorption behavior of dyes onto biochar-based biosorbents. The authors have broadly reviewed the factors influencing the biosorption process and the mechanisms describing the biosorption behaviors of the biochar. The current study was devoted to estimating and identifying Fe-doped AC prepared from Iraqi EDB that may be used for furfural efficient elimination. The prepared adsorbent was identified by scanning electron microscopy (SEM), X-ray diffraction (XRD), and Fourier-transform infrared spectroscopy (FTIR) techniques. The capability of the improved adsorbent for furfural elimination in synthetic wastewater of the Al-Doura petroleum refinery in Baghdad was estimated through kinetic, thermodynamic, and equilibrium studies with investigating the key parameters such as adsorbent loading, temperature, contact time, furfural loading, initial pH, and mixing speed. A regression model would be developed for the percentage removal of furfural experimentally obtained as a function of operating parameters.

2. Material and methods

2.1. Materials

Anhydrous ferrous sulfate ($FeSO_4$) powder (purity > 98%) was supplied by Jinan ZZ International, China. HCl (36%) and H_2SO_4 (98%), and NaOH flakes (purity > 98%) were purchased from Merck Inc. (Germany). ($NaHCO_3$) white powder (brand food grade > 99%) was purchased from Weifang Haizhiyuan Chemistry and Industry, China. Deionized water (DW) was obtained from the local market.

2.1. Methods

2.2.1. Adsorbent synthesis

The EDB fibers were scrubbed with boiling distilled water (DW) to eliminate impurities and dehydrated in an oven at 75°C for 10 h. The dehydrated fibers were crushed utilizing a ball mill (Model: TOB-DSP-LBPBM05A, China) to an extent ≤0.1 mm, and then scrubbed with a 0.5 M hydrochloric acid solution to eliminate salts presented in its pores. Then, the smashed fibers were frequently scrubbed with the DW to eliminate acidic remnants till the filtered water was transparent. The solid sample was dehydrated at 105°C for 24 h to vaporize organic impurities and then treated with 2 M sulfuric acid for 3 h at the ambient conditions. Then the solid precipitate was fully scrubbed by DW to eliminate the remnant acid absorbed. Within 10 h the solid was cured with 1 wt.% aqueous sodium bicarbonate. The solid was scrubbed with DW again till neutralization was done. The solid was placed in an N_2 purging oven (Model: K-4RS-NP, from Keen Ovens, USA) at 450°C. The calcined sample was chilled to ambient temperature and scrubbed with DW, then dehydrated for 2 h at 110°C. The prepared AC was stored in a sealed can for analysis. 0.1 mol·L^{-1} $FeSO_4$ solution was made, afterward, 10 g of the synthesized AC was added to 200 mL of this solution. The mixture was stirred at 500 rpm using a hotplate magnetic stirrer for 1 h at 50°C. At mixing, a 2 M of caustic soda solution was put on till a pH of 11 was obtained. Finally, the mixture was cooled to ambient temperature for 12 h. The precipitate was filtered and scrubbed frequently with DW.

2.2.2. Characterization of adsorbent

Energy-dispersive X-ray spectroscopy (EDX) images were conducted for samples of fine particles utilizing a Shimadzu XRD-6000 powder diffractometer with Cu-Ka radiation (k = 1.5418 Å), (40 kV, 30 mA) over the 2θ scan of 10°–80°. The surface functional groups were predicted

by FTIR spectrophotometer (NICOLET, Nexus 870 FTIR, USA) with a wavenumber scan rate extended from 600 to 3,500 cm^{-1}, utilizing beads of KBr including about 0.5% finely crushed dehydrated adsorbents. The surface morphology of AC was examined with SEM (Shimadzu SSX-550 instrument).

2.2.3. Furfural concentration monitoring

The percentage degradation (%R) of furfural was calculated by Eq. (1):

$$\text{Percentage degradation}\left(\%R\right)=\frac{C_i-C\left(t\right)}{C_i}\times 100 \tag{1}$$

where C_i and $C(t)$ are the furfural initial and instantaneous concentrations in (ppm), respectively. A series of furfural concentrations of 1, 2, 4, 6, 8, and 10 ppm are used to generate a calibration plot, as shown in Fig. S1, with a correlation coefficient of 0.992 and a standard error of 0.485, by utilizing a UV-Vis spectrophotometer (1100 UV-Vis spectrophotometer, China) at the wavelength of 287 nm.

The maximum adsorption capacity of Fe/AC was evaluated by carrying out adsorption runs. Various loadings (10, 20, 40, 60, and 75 $mg{\cdot}L^{-1}$) of an aqueous solution of furfural in demineralized water were made. Then 100 mL of each concentration is put into a 250 mL flask independently with 1 g of Fe/AC adsorbent and mixed by a magnetic stirrer for 2 h. The adsorbed mass of furfural at equilibrium, ($mg{\cdot}g^{-1}$) was evaluated by Eq. (2).

$$q_e=\frac{\left(C_i-C_{\text{ie}}\right)V}{W} \tag{2}$$

where C_i and C_{ie}: furfural loading at initial and at its corresponding equilibrium ($mg{\cdot}L^{-1}$), respectively, V: volume of the liquid phase utilized, and W: adsorbent quantity utilized (g).

2.2.4. Experimental design

The arrangement of experiments was planned by utilizing the factorial method in the present work, due to its accuracy [20]. Table 1 records the process variables (F) with their levels (L).

3. Results and discussion

3.1. Identification of the synthesized adsorbent

3.1.1. EDX analysis

Surface chemistry is the key variable for estimating the adsorption capability of AC; the synthesized AC has an elevated percentage of carbon and a lower percentage of oxygen. Fig. 1a depicts that the natural AC synthesized from the Iraqi EDB containing 60.3% wt. C, 24.6% wt. O, 2% wt. S. Additionally, the EDX spectrum of AC depicts an

Table 1
Factors and their levels selected for the present study

Level	pH	Furfural conc. ($mg{\cdot}L^{-1}$)	Mixing time (min)	Adsorbent loading ($g{\cdot}L^{-1}$)	Mixing speed (rpm)
1	4	5	30	0.5	100
2	6	10	60	1.0	200
3	8	15	90	1.5	300
4	10	20	120	2.0	

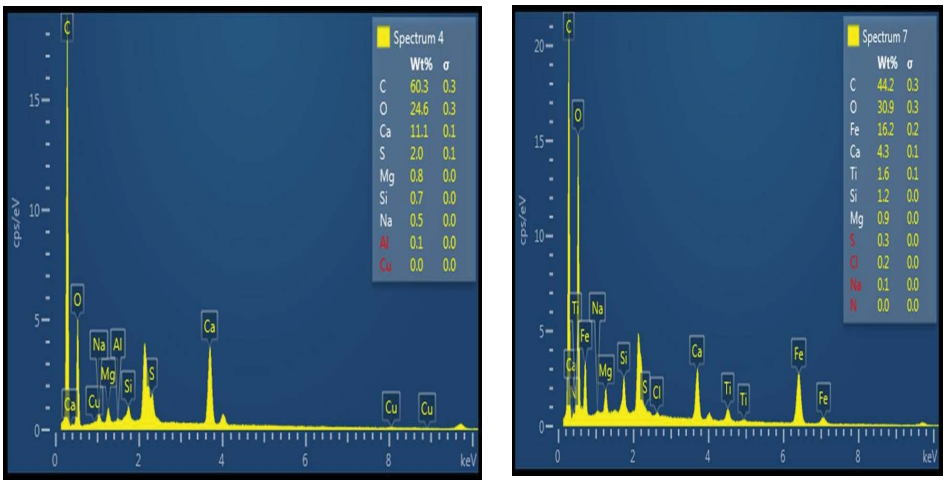

(a) (b)

Fig. 1. Energy-dispersive X-ray spectra of (a) natural activated carbon from Iraqi empty date palm bunch and (b) Fe-doping activated carbon.

extra crest that could be specified to silicon that could have formed by a plant origin. After treating with Fe solution (Fig. 1b), the content was 44.2% wt. C, 30.9% wt. O, 16.2% wt. Fe, and 1.2% wt. Si. These values reveal the effective Fe deposition onto AC particles and almost perfect oxidizing of Fe ions to Fe oxides. This outcome also detected that C and O participate largely in the elemental content of all biomasses, which is due to the organic nature of lignocellulosic remnants. Lodeiro et al. [21] found that adsorbents doped with metal have the capacity to join with many types of chemical groups like carboxyl, hydroxyl, ketone, etc. Their harmony for bonding counts on parameters such as the number of active sites, their approachability, chemical structure, and the harmony between connected sites and other ions.

3.1.2. FTIR analysis

The FTIR image of the synthesized AC before being impregnated with Fe is seen in Fig. 2a. The image depicts 4 main sorption ranges at 2,890–3,490 cm^{-1}, 1,290–1,748 cm^{-1}, 950–1,249 cm^{-1}, and 448–749 cm^{-1}. A wideband with the highest peak is observed at 2,917 cm^{-1}. The band at 3,350 cm^{-1} is attributed to the sorption of H_2O droplets as the outcome of an O–H stretching band of OH collections and soaking H_2O, whereas the band at 2,917 cm^{-1} is due to C–H interrelation on the AC surface. In the extent 1,290–1,748 cm^{-1}, amides can be recognized on the AC which has a pair of crests between 1,729 and 1,369 cm^{-1}. These functional collections were gained through the stimulation operation as an outcome of the existence of NH_3 and primary amines that are commonly presented in the sediment. Additionally, the region at 1,520 cm^{-1} could be due to the aromatic C–C stretching vibration. The pair of crests at 1,130–1,148 cm^{-1} produces the imprint of this AC. The squeaky sorption band at 1,130 cm^{-1} is due to either Si–O [22] or C–O stretching in OH collections [23,24]. The band at 1,148 cm^{-1} can also be combined with ether C–O symmetric and asymmetric stretching vibration (–C–O–C– ring) [25]. This band could also be due to the antisymmetric Si–O–Si stretching band as an outcome of presenting Al_2O_3 and SiO_2 comprising metals within the sediments [26]. The crest at 678 cm^{-1} is due to the plane of the C–H bending band. Also, these spectra were also proposed to be attributed to alkaline collections of cyclic ketones and their derivatives appended through the stimulation process [23,27].

On the other hand, for the Fe/AC images (Fig. 2b), the peak at 2,350 cm^{-1} is due to aromatic –C–C. The powerful –C–O band at 932 cm^{-1} is attributed to the $–OCH_3$ groups specified by the existence of the lignin collection in the EDB fiber which is the distinctive peak of polysaccharides. The band at 1,558 cm^{-1} in Fe/AC may be attributed to asymmetric stretching of the –C–O bond, stretching of aromatic –C–C bond, or attributed to amide stretching. In Fe/AC, the sorption crest at 3,347 cm^{-1} may be due to –NH/–OH stretching denoting the presence of free and intermolecular bonded OH groups attributed to alcoholic or phenolic functions and an amine group. Additionally, Fig. 3b shows different peaks at 1,560 and 453 cm^{-1} that could be caused by

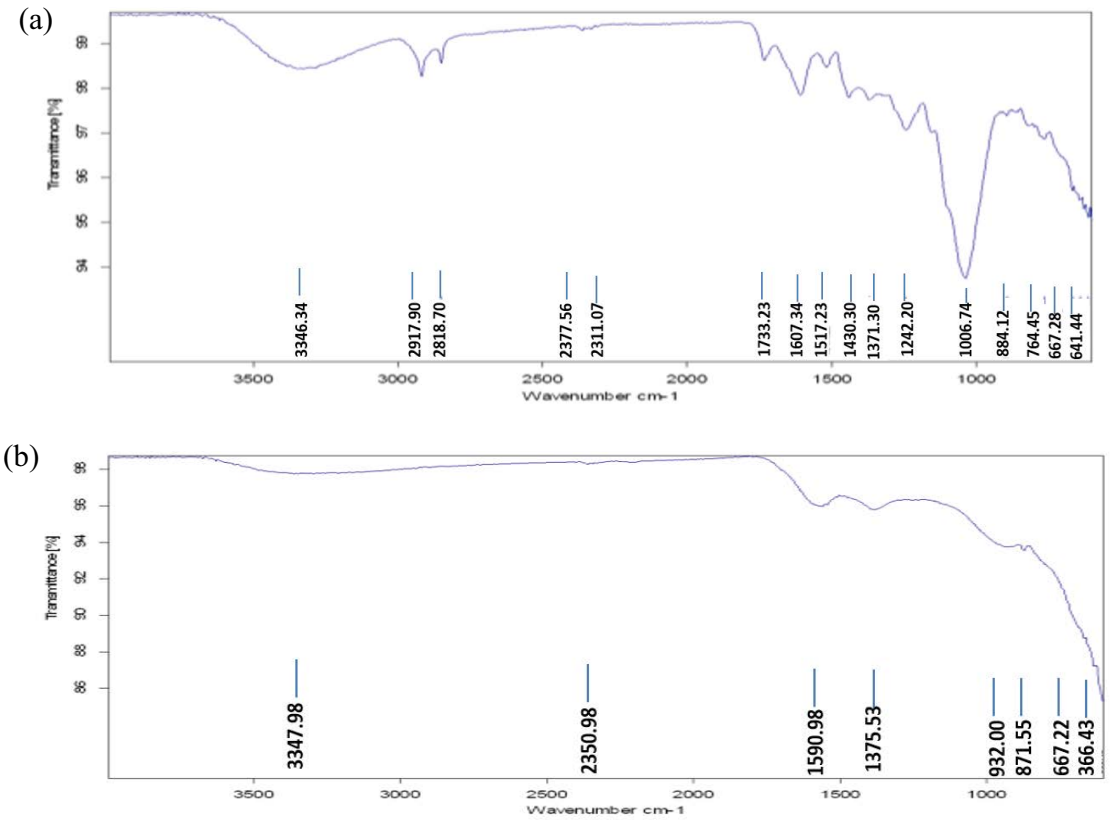

Fig. 2. Fourier-transform infrared spectra of (a) activated carbon before doping and (b) Fe/AC after doping with Fe.

the vibration mode of C=C bonding in activated carbon [28] and Fe–C bond, respectively [29].

3.2. Adsorption capacity

Fig. 3 illustrates the experimental outcomes of the adsorbed furfural at equilibrium on Fe/AC. Results observed in Fig. 4 evidence the high adsorption performance of the prepared Fe/AC and its ability to remove molecules from polluted water streams with equal efficiency. Furthermore, these high capacities prove that adsorption is not restricted to the narrow microporosity of the activated carbon but involves the entire pore system.

3.3. Effect of operating variables on adsorption efficiency

3.3.1. Influence of pH

Fig. 4 illustrates the variation of furfural percentage removal (%R) against pH at (C_i = 10 mg·L^{-1}) with AC and Fe/AC, respectively over a pH extent of 2 to 11. Fig. 4 shows that pH = 6 is optimum for the sorption of furfural over both AC and Fe/AC. Moreover, Fig. 4 depicts that as pH varied from 2 to 6 the %*R* increased from 47% to 78% for Fe/AC and from 39% to 63% for AC. However, different behavior was observed when pH increased from 6 to 11, the furfural removal decreased from 78% to 68% for Fe/AC, and 63% to 52% for AC. Results of Fig. 4 revealed that the AC doped with Fe made an average percentage removal of furfural of 14% more than that of AC. This behavior can be explained from the van der Waals forces point of view. At pH < pH_{pzc}, the Fe/AC had a positive charge, and at pH > pH_{pzc}, it had a negative charge. As a result, in solutions with a pH < 6.0, the adsorbent particles had a positive charge at their surface, while the furfural molecules were negatively charged. As the pH reduces, due to the increasing of the ($^+$H) ions in the solution, the formation of an electrostatic attraction between the ($^+$H) ion and the furfural molecules increases that eventually increasing the adsorption rate as well. On the other hand, adsorbent particles had a negative charge due to pH > 6.0, so the anionic furfural and the adsorbent repelled. The present results agree with previous published data of [30,31], and [5]. Moreover, it can be deduced that pH impacts the framework stability of furfural and, subsequently its loading. These results confirmed that the furfural solution is stabilized at pH = 6, and the solution turns unstable if pH is either raised or reduced. Parpot et al. [32] reported that furfural can be turned into furfurylic alcohol or oxidized into furoic acid:

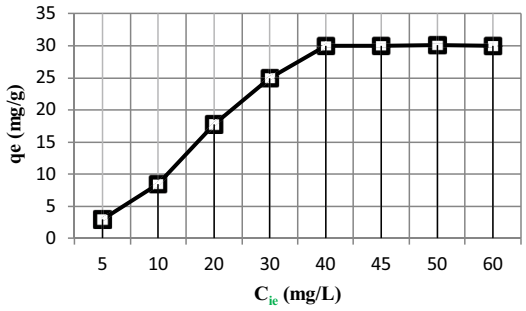

Fig. 3. Plot of furfural adsorption at equilibrium on Fe/AC sample (30°C, C_i = 10–75 mg·L^{-1}, and 125 min).

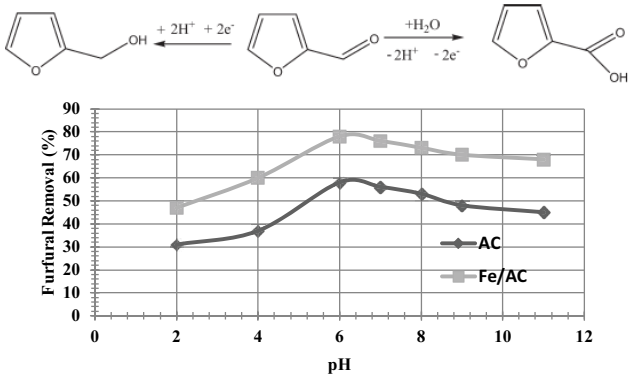

Fig. 4. Variation of furfural removal against pH at (C_i = 10 mg·L^{-1}, t = 125 min, and adsorbent loading of 1.5 g·L^{-1}).

3.3.2. Effect of adsorbent dosage

Fig. 5 depicts the influence of contact time on the removal of furfural at different loadings (m) of Fe/AC. As can be seen in Fig. 5, the increase in adsorbent quantity, mostly, enhances the adsorption because of the larger surface area and having more active sites ready for adsorption. It can be shown that at each adsorbent loading the trend of furfural removal rate increases rapidly at the first 20 min of operation then it becomes slower as the work goes on. This may be attributed to the active sites which become continuously occupied by furfural molecules with operating time. Moreover, the experimental results revealed that as $m \geq 1.5$ g·L^{-1}, the removal competence was nearly steady, suggesting an optimum value of 1.5 g·L^{-1} for adsorbent loading with keeping other operating parameters unchanged. The adsorbent surface becomes saturated with furfural for $m < 1.5$ g·L^{-1}, and the residual concentration in the solution is large.

3.4. Adsorption isotherm models

3.4.1. Langmuir isotherm

The creation of monolayer adsorption with equal heat of adsorption on the surface is assumed in this model [33]. Eq. (3) represents Langmuir isotherm [34],

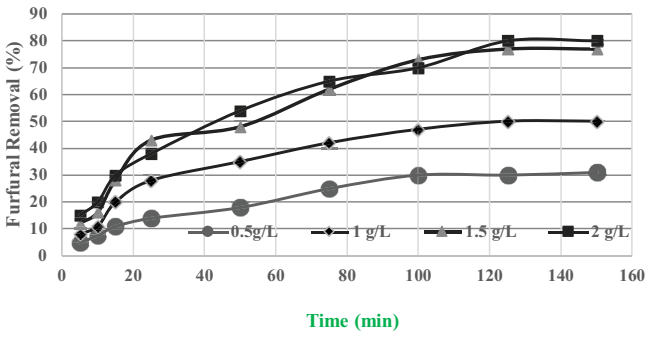

Fig. 5. Effect of contact time on furfural removal at different adsorbent dosing of Fe/AC.

$$q_e = \frac{C_e q_m b}{bC_e + 1} \quad (3)$$

where q_m is the Langmuir constant associated with adsorption capacity (mg·g^{-1}), b: constant refers to the adsorption energy (L·mg^{-1}). The slope of the linear plot of C_e/q_e vs. C_e may be used to determine the constants q_m and b from Eq. (3).

3.4.2. Freundlich isotherm

The surface energy is defined by using the equation provided by [35]:

$$\ln q_e = \ln K_f + \frac{1}{n}\ln C_e \quad (4)$$

where K_f is a constant related to the sorbet's adsorption capacity, and n is the adsorption intensity based on n's value poor adsorption, moderate adsorption, and good adsorption are observed when the value of $n < 1$, n = 1–2, and n = 2–10, respectively [36].

3.4.3. Temkin isotherm

Temkin's isotherm model may be represented in a linearized form as [37]:

$$q_e = b\ln K_t + B\ln C_e \quad (5)$$

where K_t: the maximum binding energy is represented by the equilibrium binding constant (L·g^{-1}), $B = RT/b$ is the Temkin constant (J·kJ^{-1}), b: is the adsorption heat (kJ·mol^{-1}), R: is the universal gas constant (8.314 J·mol^{-1}·K^{-1}), and T: is the absolute temperature (K).

3.5. Adsorption equilibrium study

The Langmuir and Freundlich equations are widely used for isotherm modeling. The isotherm constants for the isotherms studied, and the correlation coefficient (R^2) are cited in Table 2. The R^2 values for the Langmuir isotherm are closer to unity in comparison to the values obtained for the other two isotherms. As can be observed from Table 2, Langmuir is the best-fit isotherm equation for the adsorption of furfural on Fe/AC at all temperatures.

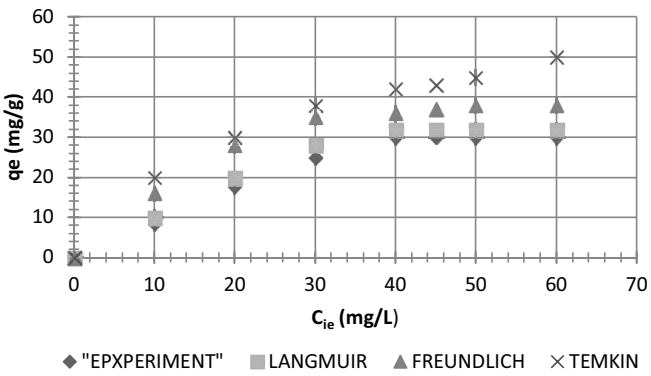

Fig. 6. Comparing of various isotherm models for the adsorption of furfural onto Fe/AC at 308 K.

Fig. 6 presents how well the three isotherms fit the data for the furfural-Fe/AC system. The data in Table 2 also indicate that the values of q_m and K_f decreased with an increase in temperature confirming the exothermic nature of the overall sorption process for furfural-Fe/AC system. Since $n > 1$, furfural is favorably adsorbed by the Fe/AC at all temperatures. The K_f value can be taken as a relative indicator of the adsorption capacity of Fe/AC for a narrow subregion having equally distributed energy sites for the sorption of furfural. The magnitude of K_f also showed a lower uptake of furfural at higher temperatures indicating the exothermic nature of the adsorption process.

3.6. Adsorption kinetics

3.6.1. First-order kinetic

The pseudo-first-order kinetic model was used to analyze the kinetic data. The model's linear form is provided in Eq. (6) [38,39]:

$$\log\left(q_e - q_t\right) = \log q_e - \frac{K_1}{2.303}t \quad (6)$$

where q_e is the amount of sulfur adsorbed at equilibrium (mg·g^{-1}), q_t is the amount of sulfur absorbed over time (mg·g^{-1}), and K_1 is the constant equilibrium rate of the pseudo-first-order model (min^{-1}). The slope and intercept of the linear plot may be used to calculate the rate constant K_1, the adsorbed quantity at equilibrium (q_e), and the values of R^2.

3.6.2. Second-order kinetic

The pseudo-second-order kinetic interaction is represented in Eq. (7) [40]:

$$\frac{t}{q_t} = \frac{1}{K_2 q_e^2} + \frac{1}{q_e} \quad (7)$$

Table 2
Isotherm parameters for the removal of furfural by Fe/AC (t = 100 min, C_i = 0–10 mg·L^{-1}, m = 1.5 g·L^{-1})

Langmuir			
T (K)	b (L·mg^{-1})	q_m (mg·g^{-1})	R^2
298	22.18	0.053	0.999
303	21.63	0.051	0.987
308	20.04	0.045	0.999
Freundlich	K_f [(mg·g^{-1})((L·mg^{-1})$^{1/n}$)]	n^{-1}	R^2
298	4.05	0.283	0.976
303	4.00	0.281	0.964
308	3.90	0.277	0.977
Temkin	K_t (L·mg^{-1})	B (kJ·mol^{-1})	R^2
298	0.79	3.82	0.937
303	0.61	3.92	0.912
308	0.63	3.66	0.951

where K_2 is rate constant of the pseudo-second-order for sorption (g·mg^{-1}·min^{-1}). (t/q_t) was plotted against the time to obtain K_2 and q_e for the pseudo-second-order kinetic model.

3.6.3. Intraparticle diffusion

The possibility of intraparticle diffusion is represented by this model, as seen in Eq. (8) [41]:

$$q_t = K_p t^{0.5} + I \quad (8)$$

where K_p denotes the constant intraparticle diffusion rate (mg·g^{-1}·min$^{-0.5}$) and I denotes the constant intraparticle diffusion.

Pseudo-first-order, pseudo-second-order, and intraparticle models were used to fit the adsorbent, and the results are listed in Table 3. The fit achieved by the pseudo-first-order model of kinetic adsorption is shown in Fig. 7a. As can be observed, the R^2 = 0.9602, indicates that the pseudo-first-order model fits well with the experimental kinetic data.

The plot of the pseudo-second-order model, which gave R^2 = 0.8339, is shown in Fig. 7b; this value is low when compared to the pseudo-first-order model. This confirms that the adsorption kinetics don't really fit the adsorbent's experimental kinetic data.

Table 4
Thermodynamics parameters for the adsorption of furfural by Fe/AC (t = 2 h, C_i = 10–80 mg·L^{-1})

Temperature (K)	B × 10^{-3} (L·kg^{-1})	ΔG° (kJ·mol^{-1})	ΔH° (kJ·mol^{-1})	ΔS° (J·mol^{-1}·K^{-1})
298	1.062	–17.263	–13.24	13.5
303	0.860	–17.021		
308	0.745	–16.934		
313	0.686	–16.995		

Table 3
Parameters of kinetic models

Pseudo-first-order	R^2		K_1		q_e (mg·g^{-1})	
	0.9602		0.0001		5.3817	
Pseudo-second-order	R^2		K_2		q_e (mg·g^{-1})	
	0.8339		0.0007		9.98	
Intraparticle diffusion	Characteristics of the overall intraparticle diffusion					
	R^2		K_i		C (mg·g^{-1})	
	0.8788		0.029		1.0313	
	Kinetics for different sections of the intraparticle diffusion					
	Section 1			Section 2		
	R^2_1	K_{i1}	C_1 (mg·g^{-1})	R^2_2	K_{i2}	C_2 (mg·g^{-1})
	0.943	0.0607	0.02	0.903	0.0157	3.02

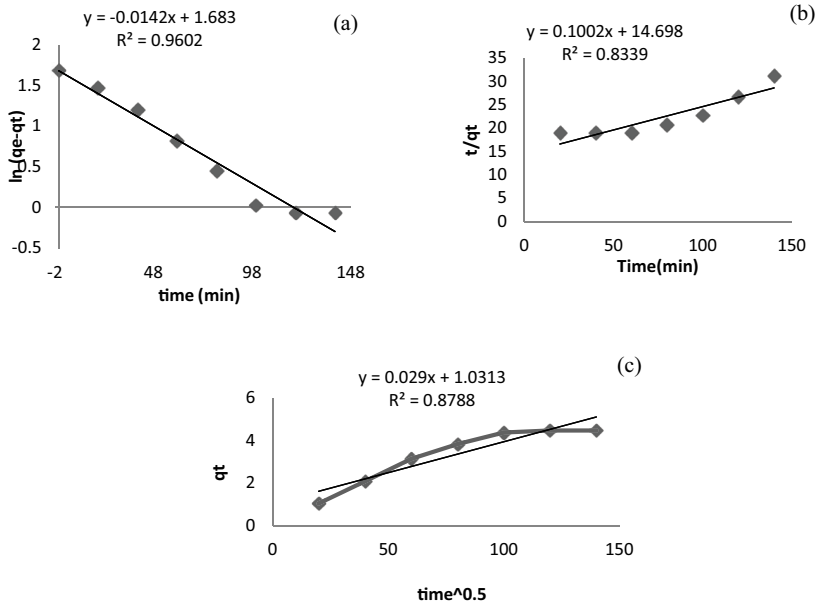

Fig. 7. (a) Pseudo-first-order, (b) pseudo-second-order, and (c) intraparticle diffusion kinetic models).

Table 5
Design of experiments with the experimental results of the furfural percentage removal

A: pH	*B*: initial conc.	*C*: mixing time	*D*: adsorbent loading	*E*: mixing speed	Percentage furfural removal (experimental results)
	($mg \cdot L^{-1}$)	(min)	($g \cdot L^{-1}$)	(rpm)	
4	15	30	0.5	100	30
4	5	30	0.5	300	34
10	15	90	0.5	100	50
4	5	90	1.5	300	44
10	5	30	1.5	300	60
7	10	60	1	200	57
7	10	60	1.5	200	73
7	10	60	1	200	54
7	10	60	1	200	55.6
10	15	30	0.5	300	51.8
10	5	90	0.5	300	56
4	5	30	0.5	100	32
4	15	30	1.5	100	43
10	10	60	1	200	49
10	15	90	1.5	100	54
4	15	90	1.5	300	47
7	10	60	1	200	53
10	5	30	0.5	100	52
4	5	90	1.5	100	44
4	5	90	0.5	100	29
7	5	60	1	200	57
4	15	30	0.5	300	34
10	15	90	1.5	300	55
7	10	60	1	200	53
4	5	90	0.5	300	33.6
4	15	90	0.5	300	29
4	15	30	1.5	300	47
10	5	30	0.5	300	57
10	15	30	0.5	100	50
7	10	60	1	100	56
7	10	90	1	200	52.5
7	10	60	1	200	57
7	10	60	1	200	53
4	5	30	1.5	100	43
7	10	30	1	200	50
10	5	90	1.5	100	58
4	10	60	1	200	35
10	5	90	0.5	100	54
4	15	90	1.5	100	46
4	5	30	1.5	300	48
7	10	60	1	300	59.7
10	15	90	0.5	300	53
7	10	60	1	200	57
10	5	90	1.5	300	61
10	15	30	1.5	100	55
10	5	30	1.5	100	54.7
4	15	90	0.5	100	31
7	10	60	0.5	200	64

In Fig. 7c, the plot of the intraparticle diffusion model is presented; two sections are apparent, each indicating distinct adsorption behavior. As seen in the first linear section, the adsorption capacity varies rapidly over time until it achieves equilibrium. This implies that the control step may be the diffusion of the boundary layer. Experimental data points were the horizontal line in the second section, indicating that equilibrium was attained and that intraparticle diffusion was taking place. The values of K_1 and K_2 are presented in Table 3. Moreover, kinetics for different sections of the intraparticle diffusion has been also calculated, and listed in Table 3.

3.7. Thermodynamic study

Thermodynamic parameters like enthalpy ($\Delta H°$, kJ·mol^{-1}), standard entropy ($\Delta S°$, kJ·mol^{-1}·K^{-1}), and changes in the Gibb's free energy ($\Delta G°$, kJ·mol^{-1}) were evaluated to test the sorption operation by utilizing Eqs. (9)–(12) [42,43].

$$\beta = \frac{C_i - C_{ie}}{C_{ie}} \tag{9}$$

$$\ln\beta = -\frac{\Delta H°}{RT} + \frac{\Delta S°}{R} \tag{10}$$

$$\Delta G° = -RT\ln\beta \tag{11}$$

$$\Delta G° = \Delta H° - T\Delta S° \tag{12}$$

where β is the equilibrium constant, R (=8.134 J·mol^{-1}·K^{-1}), and T (K) is the absolute temperature. Plotting of (lnβ vs. 1/T) represents a straight line; amounts of $\Delta H°$ and $\Delta S°$ were obtained from the inclination and the line intercept, respectively.

The ΔG of the sorption operation is linked to the equilibrium parameter β by the van't Hoff equation [Eq. (4)]. Moreover, ΔG is also related to the ΔS and ΔH to obtain:

$$-\frac{\Delta G°}{RT} = -\frac{\Delta H°}{RT} + \frac{\Delta S°}{R} \tag{13}$$

The positive value of $\Delta S°$ indicates an excess in the grade of freedom of the adsorbed species. Table 4 lists the thermodynamics parameters for the sorption of furfural by Fe/AC. The negative $\Delta H°$ value assures the exothermic sate of the total-sorption operation. The heat of sorption amounts between 0–20 kJ·mol^{-1} is commonly presumed to point out the physical state of sorption. For furfural sorption over Fe/AC, the value of $\Delta H°$ was –13.24 kJ·mol^{-1}. It is clear from the relatively low value of $\Delta H°$ that the physio-sorption principally participates in the sorption operation. The sign of ΔG° values was negative revealing the spontaneity and feasibility of the sorption operation.

3.8. Regression model

Table 5 lists the values of the operating parameters of each experiment with the corresponding percentage removal of furfural experimentally obtained.

Values listed in Table 5 have been used to explore the association between the furfural removal efficiency (R%) and the process variables. Based on the regression analysis technique, using the least squares approach utilizing MINITAB software, Eq. (13) below reveals the objective function (i.e., adsorption efficiency) as a function of operating parameters with a correlation coefficient (R^2) of 0.9875 and standard of deviation = 1.18%:

$$\begin{aligned}\text{RT\%} = {} & -45.51 + 27.61A - 1.58B - 75.52D - 0.0144E - 1.643A^2 \\ & + 0.00615C^2 + 46.87D^2 - 0.0564AB + 1.652AD\end{aligned} \tag{14}$$

where A, B, C, D, and E refer to initial pH, initial furfural concentration (mg·L^{-1}), mixing time (min), adsorbent loading (g·L^{-1}), and mixing speed (rpm), respectively.

A positive sign in the preceding equation implies that increasing the value of the variable leads to an increase in furfural removal. Concurrently, the negative sign depicts that the value of the variable results in a decrease in furfural removal. The interaction effect is represented by two variables, whereas the square effect is represented by the second-order term of the variables. The response surface method was applied to define the significant factors that affect the adsorption process. It was found that the effects of five variables take the following sequence:

pH > initial concentration > adsorbent dose > mixing time > mixing speed.

4. Conclusion

In the current study, EDB fibers have been used as a precursor to synthesize an activated carbon and Fe-doped activated carbon (Fe/AC) for furfural removal from synthetic wastewater discharged from the Al-Doura refinery in Baghdad. Moreover, Fe-doped activated carbon (Fe/AC) was also prepared. Different key parameters such as adsorbent loading, contact time, furfural loading, initial pH, and mixing speed were used to investigate their effects on the effectiveness of AC and Fe/AC for furfural removal. SEM, XRD, and FTIR techniques confirmed the efficient preparation process of adsorbents. Experimental results showed that after 125 min. of contact time a percentage removal efficiency of 80% and 58% with absorption capacities of 27.04 and 16.80 mg·g^{-1} was attained by using Fe/AC, and AC, respectively at optimum initial pH of 6. Results showed that the pseudo-first-order fitted well with the system kinetics. Moreover, the Langmuir isotherm model agreed well with the adsorption equilibrium system. For furfural adsorption over Fe/AC at 298 K, the values of $\Delta G°$, $\Delta H°$, and $\Delta S°$ were –17.263, –13.24, and 16.3 kJ·mol^{-1}, respectively. Results of the thermodynamic parameters (i.e., $\Delta G°$, $\Delta H°$, and $\Delta S°$) revealed that the process was spontaneous, exothermic, and with an increase in the degree of freedom of the adsorbed species at the liquid–solid interface during the sorption operation.

Acknowledgments

The authors are grateful to the University of Technology for providing space and facilities. Thanks are also due Al-Turath University College for the assistance.

Competing interests

The authors have declared they have no conflict of interest with any organization or any person.

References

[1] S. Singh, V.C. Srivastava, I.D. Mall, Fixed-bed study for adsorptive removal of furfural by activated carbon, Colloids Surf., A, 332 (2009) 50–56.

[2] W.D. Yang, P.L. Li, D.C. Bo, H.Y. Chang, The optimization of formic acid hydrolysis of xylose in furfural production, Carbohydr. Res., 357 (2012) 53–61.

[3] EPA, Pesticide Fact Sheet (Office of Prevention, Pesticide and Toxic Substance), Contract No: 7505P, U.S. Environmental Protection Agency, 2006.

[4] OSHA, Occupational Safety and Health Guideline, Labor USD, Washington D.C., 1992.

[5] R.N. Ghazy, I.K. Shakir, Furfural removal from refinery wastewater by adsorption on commercial activated carbon, J. Pet. Res. Stud., 12 (2022) 116–136.

[6] A.S. Alsaqqar, M.S. Salman, W.M. Abood, D.F. Ali, Furfural degradation in wastewater by advanced oxidation process using UV/H_2O_2, Iraqi J. Chem. Pet. Eng., 16 (2015) 9–17.

[7] M.T. Khan, J. Krümpel, D. Wüst, A. Lemmer, Anaerobic degradation of individual components from 5-hydroxymethylfurfural process-wastewater in continuously operated fixed bed reactors, Processes, 9 (2021) 677, doi: 10.3390/pr9040677.

[8] L.Y. Mao, L. Zhang, N.B. Gao, A.M. Li, $FeCl_3$ and acetic acid co-catalyzed hydrolysis of corncob for improving furfural production and lignin removal from residue, Bioresour. Technol., 123 (2012) 324–331.

[9] M.R. Fahmi, C.Z.A. Abidin, N.R. Rahmat, Characteristic of Color and COD Removal of Azo Dye by Advanced Oxidation Process and Biological Treatment, 2011 International Conference on Biotechnology and Environment Management IPCBEE Vol. 18, IACSIT Press, Singapore, 16–18 Sept., 2011.

[10] T. Yang, A. Lua, Characteristics of activated carbons prepared from pistachio-nut shells by physical activation, J. Colloid Interface Sci., 267 (2003) 408–417.

[11] D. Mohan, C.U. Pittman, Activated carbons and low-cost adsorbents for remediation of tri- and hexavalent chromium from water, J. Hazard. Mater., 137 (2006) 762–811.

[12] M.F. Abid, H.S. Yasser, A.H. Bilal, T.J. Farah, Glucose production from Iraqi date-palm empty fruit fibers, J. Xian Univ. Archit. Technol., XII (2020) 124–141.

[13] W. Chen, R. Parette, J. Zou, F.S. Cannon, B.A. Dempsey, Arsenic removal by iron-modified activated carbon, Water Res., 41 (2007) 1851–1858.

[14] V. Fierro, G.C. Muniz, G. Gonzalez, M.L. Ballinas, A. Celzard, Arsenic removal by iron-doped activated carbons prepared by ferric chloride forced hydrolysis, J. Hazard. Mater., 168 (2009) 430–437.

[15] A.M. Cooper, K.D. Hristovski, T. Möller, P. Westerhoff, P. Sylvester, The effect of carbon type on arsenic and trichloroethylene removal capabilities of iron (hydr) oxide nanoparticle-impregnated granulated activated carbons, J. Hazard. Mater., 183 (2010) 381–388.

[16] Z. Wang, M. Shi, J. Li, Z. Zheng, Influence of moderate pre-oxidation treatment on the physical, chemical and phosphate adsorption properties of iron-containing activated carbon, J. Environ. Sci., 26 (2014) 519–528.

[17] A. Chatla, I.W. Almanassra, L. Jaber, V. Kochkodan, T. Laoui, H. Alawadhi, M.A. Atieh, Influence of calcination atmosphere on Fe-doped activated carbon for the application of lead removal from water, Colloids Surf., A, 652 (2022) 129928, doi: 10.1016/j.colsurfa.2022.129928.

[18] A. Soudani, L. Youcef, L. Bulgariu, S. Youcef, K. Toumi, N. Soudani, Characterizing and modeling of oak fruit shells biochar as an adsorbent for the removal of Cu, Cd, and Zn in single and in competitive systems, Chem. Eng. Res. Des., 188 (2022) 972–987.

[19] S. Praveen, J. Jegan, T.B. Pushpa, R. Gokulan, L. Bulgariu, Biochar for removal of dyes in contaminated water: an overview, Biochar, 4 (2022) 3–16.

[20] K. Krishnaiah, P. Shahabudeen, Applied Design of Experiments and Taguchi Methods, PHI Learning Private Limited, New Delhi, 2012.

[21] P. Lodeiro, J.L. Barriada, R. Herrero, M.E.S. de Vicente, The marine macroalga *Cystoseira baccata* as biosorbent for Cd(II) and Pb(II) removal: kinetic and equilibrium studies, Environ. Pollut., 142 (2006) 264–273.

[22] A. Misra, P.K. Tyagi, M.K. Singh, D.S. Misra, FTIR studies of nitrogen doped carbon nanotubes, Diamond Relat. Mater., 15 (2006) 385–388.

[23] S.H. Park, S. McClain, Z.R. Tian, S.L. Suib, C. Karwacki, Surface and bulk measurements of metals deposited on activated carbon, Chem. Mater., 9 (1997) 176–183.

[24] A.A. Attia, W.E. Rashwan, S.A. Khedr, Capacity of activated carbon in the removal of acid dyes subsequent to its thermal treatment, Dyes Pigm., 69 (2006) 128–136.

[25] G. Calzaferri, R. Imhof, *In-situ* attenuated total reflection FTIR investigations of H_2O, $HSiCl_3$ and $Co_2(CO)_8$ on ZnSe in the range 600–4,000 cm^{-1}, Spectrochim. Acta, Part A, 52 (1996) 23–28.

[26] J. Guo, A. Lua, Textural and chemical characterizations of activated carbon prepared from oil-palm stone with H_2SO_4 and KOH impregnation, Microporous Mesoporous Mater., 32 (1999) 111–117.

[27] R. Lapuente, F. Cases, P. Garcés, E. Morallón, J.L. Vázquez, A voltammeter and FTIR–ATR study of the electro polymerization of phenol on platinum electrodes in carbonate medium: influence of sulfide, J. Electroanal. Chem., 451 (1998) 163–171.

[28] A.S. Yasin, J. Jeong, I.M.A. Mohamed, C.H. Park, C.S. Kim, Fabrication of N-doped &SnO_2-incorporated activated carbon to enhance desalination and bio-decontamination performance for capacitive deionization, J. Alloys Compd., 729 (2017) 764–775.

[29] I.M.A. Mohamed, A.S. Yasin, C. Liu, Synthesis, surface characterization and electrochemical performance of ZnO/activated carbon as a supercapacitor electrode material in acidic and alkaline electrolytes, Ceram. Int., 46 (2020) 3912–3920.

[30] A.K. Sahu, V.C. Srivastava, I.D. Mall, D.H. Lataye, Adsorption of furfural from aqueous solution onto activated carbon: kinetic, equilibrium and thermodynamic study, Sep. Sci. Technol., 43 (2008) 1239–1259.

[31] M. Fazlzadeh, M. Ansarizadeh, M. Leili, Data of furfural adsorption on nano zero valent iron (NZVI) synthesized from Nettle extract, Data Brief, 16 (2018) 341–345.

[32] P. Parpot, A.P. Bettencourt, G. Chamoulaud, K.B. Kokoh, E.M. Belgsir, Electrochemical investigations of the oxidation-reduction of furfural in aqueous medium: application to electrosynthesis, Electrochim. Acta, 49 (2004) 397–403.

[33] K.Y. Foo, B.H. Hameed, Insights into the modeling of adsorption isotherm systems, Chem. Eng. J., 156 (2010) 2–10.

[34] I. Langmuir, The constitution and fundamental properties of solids and liquids. II. Liquids, J. Am. Chem. Soc., 39 (1917) 1848–1906.

[35] A.A. Sabri, T.M. Albayati, R.A. Alazawi, Synthesis of ordered mesoporous SBA-15 and its adsorption of methylene blue, Korean J. Chem. Eng., 32 (2015) 1835–1841.

[36] Y. Yao, B. He, X. Feifei, C. Xiaofeng, Equilibrium and kinetic studies of methyl orange adsorption on multiwalled carbon nanotubes, Chem. Eng. J., 170 (2011) 82–89.

[37] I.H. Khalaf, F.T. Al-Sudani, A.A. AbdulRazak, T. Aldahri, S. Rohani, Optimization of Congo red dye adsorption from wastewater by a modified commercial zeolite catalyst using response surface modeling approach, Water Sci. Technol., 83 (2021) 1369–1383.

[38] G.I. Danmaliki, T.A. Saleh, Effects of bimetallic Ce/Fe nanoparticles on the desulfurization of thiophenes using activated carbon, Chem. Eng. J., 307 (2017) 914–927.

[39] S. Lagergren, Zur theorie der sogenannten adsorption geloster stoffe, Kungliga Svenska Vetenskapsakademiens. Handlingar, 24 (1898) 1–39.

[40] A.A. AbdulRazak, S. Rohani, Sodium dodecyl sulfate modified Fe_2O_3/molecular sieves for removal of rhodamine B dyes, Adv. Mater. Sci. Eng., 10 (2018) 1–10.
[41] B. An, Cu(II) and As(V) adsorption kinetic characteristic of the multifunctional amino groups in chitosan, Processes, 8 (2020) 1194–1209.
[42] L. Radia, B. Oumessaad, A. Hamitouche, D. André, Adsorption of hexavalent chromium by activated carbon obtained from a waste lignocellulosic material (*Ziziphus jujuba* cores): kinetic, equilibrium, and thermodynamic study, Adsorpt. Sci. Technol., 36 (2018) 1–34.
[43] M. Jain, Y. Mithilesh, K. Tomas, K.G. Vinod, S. Mika, Development of iron oxide/activated carbon nanoparticle composite for the removal of Cr(VI), Cu(II) and Cd(II) ions from aqueous solution, Water Resour. Ind., 20 (2018) 54–74.

Supporting information

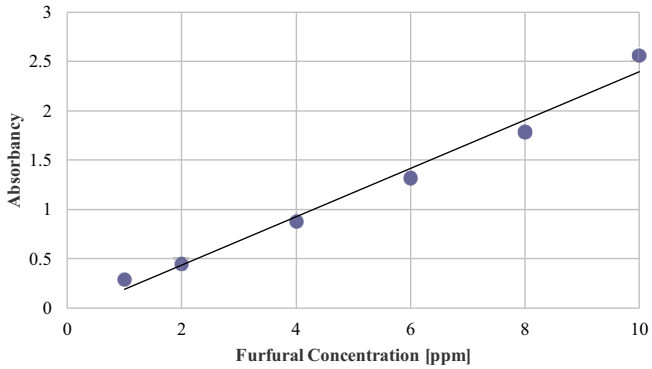

Fig. S1. Calibration curve of furfural.